Differential reach vector computations in mIPS and PMd as

revealed through HD-tDCS

Sisi Xu, Jason Gallivan, Gunnar Blohm

Centre for Neuroscience Studies, Queen's University, Kingston, ON, Canada

Corresponding author: Gunnar Blohm (gunnar.blohm@queensu.ca)

8 **Abstract**

9 Recent neural and behavioural findings provide support that the medial

10 intraparietal sulcus (mIPS) and dorsal premotor (PMd) activity reflect aspects of a

11 kinematic plan for reaching movements. However, it is unclear how these two

12 regions differentially contribute to reach planning. Here, we used high-definition

13 transcranial direct current stimulation (HD-tDCS; 4 x 1 electrode placement; 2 mA

14 for 20 min; 3 cm radius) to investigate the functional roles of mIPS and PMd in the

15 left hemisphere of humans. We examined the changes in endpoint error in reaching

16 task with different initial hand positions and different target locations spanning

17 both visual hemi-fields. Participants completed the task with (stimulation, post-

18 stimulation) and without stimulation (pre-stimulation) of individually fMRI-

19 localized cortical areas mIPS and PMd. We found a significant interaction effect

20 between initial hand position (IHP) and target position on the difference in

21 horizontal endpoint error after cathodal left mIPS stimulation and significant IHP

22 and target position main effects after cathodal left PMd stimulation, suggesting that

23 IHP and target position are not yet integrated into a movement vector at the input of

24 the mIPS, but are integrated in the input of PMd. Hence, these findings reveal a

25 distinction between mIPS and PMd in the stages of movement vector formation for

26 reaching movements and indicate that HD-tDCS is a viable method for perturbing

27 localized cortical activity to elucidate localized cortical function.

28

29

30 **Introduction**

31 To plan goal-directed reaches, we need to compute a movement plan that specifies

32 the reach goal location relative to the initial hand position (Vindras & Viviani, 1998).

33 The calculation of this difference vector is believed to occur during the

34 transformation from the initial conditions of the hand and target position into the

35 motor command (Batista, Buneo, Snyder, & Andersen, 1999), providing aspects of

36 the movement plan, i.e. amplitude and direction information for movement

37 execution (Krakauer, Pine, Ghilardi, & Ghez, 2000; Bock & Arnold, 1992). However,

38 where and how spatial information is stored and combined in the brain persist as a

39 gap in our understanding of this process.

40 A number of parietofrontal circuits are thought to be devoted to the process

41 of planning for different movement types ahead of movement execution. One

42 particular example is the dorsomedial pathway, which comprises regions relevant

43 to reaching component of reach-to-grasp actions: the medial part of IPS (mIPS), the

44 parieto-occipital junction (POJ), and the dorsal premotor cortex (PMd) (Jeannerod,

45 Arbib, Rizzolatti, & Sakata, 1995). Studies of the early component of the dorsomedial

46 pathway, the mIPS, using transcranial magnetic stimulation (TMS) tend to suggest a

47 role in encoding visual information about the initial hand position from visual cortex

48 (Vesia & Crawford, 2012) but has also been implicated in processing movement

49 direction (Davare, Zénon, Desmurget, & Olivier, 2015). Thus, there is conflicting

50 indications of a disposition upstream as opposed to downstream of the visuomotor

51 transformation.

52   The later component of the dorsomedial pathway, the PMd, also plays a role

53   in reach planning, based on delay period activity in monkey PMd which was thought

54   to represent the movement plan for reaching movements as the target location

55   selectivity was independent of choice of hand use (Cisek, 2002). Appearing to

56   complementary to the direction coding role of the mIPS, the PMd has been

57   suggested to be involved in amplitude coding (Davare, Zénon, Desmurget, & Olivier,

58   2015). Yet, potential differences between the two regions in the formation of the

59   movement vector remain to be examined. What part of the movement plan (i.e., IHP,

60   target position, or difference vector) is encoded in mIPS and PMd?

61   Transcranial direct current stimulation (tDCS) can serve as a valuable tool

62   for non-invasive and reversible modulation of cortical excitability to unravel cortical

63   structure-function relationships. A weak electrical direct current is applied to the

64   scalp to induce polarity-dependent subthreshold modulations and consequent

65   changes in cortical excitability in the underlying cortex. Anodal stimulation

66   produces neuronal depolarization and promotes neuronal excitation in the

67   stimulated cortical area while cathodal stimulation in hyperpolarization and

68   neuronal inhibition (Bindman et al. 1962; Purpura & McMurtry, 1965). The high

69   definition 4 x 1 configuration offers the ideal stimulation focality to study the

70   function of a more specific cortical area. The 4x1 HD-tDCS configuration which

71   consists of small disc electrodes arranged in a ring significantly enhances spatial

72   accuracy and precision due to the smaller electrode size, ring radius (distance

73   between centre and surround electrode), and the configuration-determined current

74   paths (Datta, Truong, Minhas, Parra, & Bikson, 2012; Datta et al, 2009). The central

75   electrode, which determines the polarity, is placed over the target and the 4

76   surrounding return electrodes are placed around it to guide current flow. It is not

77   known how HD-tDCS of mIPS or PMd may affect movement planning. To our

78   knowledge, HD-tDCS has not been applied previously in the study of motor

79   planning.

80   Here, we stimulated the mIPS and PMd in the left hemisphere and examined

81   participants' performance on a right-hand reaching task and inferred the functional

82   roles of the two areas based on performance changes. We hypothesized polarity-

83   specific behavioral effects on the basis of polarity-specific neurophysiological

84   effects, i.e., somatic depolarization (hyperpolarization) by anodal (cathodal)

85   stimulation. Our results provide evidence that HD-tDCS can modulate performance

86   in a movement planning task to reveal differences in the functional properties of

87   mIPS and PMd.

88

MATERIALS AND METHODS

Participants

Ten volunteers (age range: 20 – 39; 7 females) participated in the experiment.
Participants had normal or corrected-to-normal vision and were right handed. They
performed two tasks with their dominant right hand: an fMRI localizer session
followed by the main tDCS experiment. Participants provided written informed
consent to the experimental conditions that were approved by the Queen's
University General Board of Ethics, in compliance with the Declaration of Helsinki.

Overview of Experiment

Each participant underwent a localizer session consisting of one anatomical scan
and one functional scan. Subsequently, all subjects made 4 visits for the HD-tDCS
experiment (2 polarity x 2 sites), with a one-week interval between visits. (Note:
experiments and analyses were carried out in 2014-2016)

MRI Acquisition & Localizer Task

Imaging was conducted using a 3-Tesla Magnetom Trio scanner (Siemens Medical
Systems, Erlangen, Germany). Participants rested supine in the scanner and wore a
32-channel head coil. At the beginning of the localizer session, a 176 slice, high-
resolution T1- weighted anatomic reference volume was acquired using a 3D MP-
RAGE sequence (single shot, ascending sequence in the sagittal plane with TR =
1760 ms, TE = 2.2 ms, FoV = 256 mm, flip angle = 9°, and voxel size = 1 mm^3).

6

111   Participants were then scanned with blood oxygenation level-dependent

112   (BOLD) fMRI for the localization of the reaching network during an interleaved

113   center-out pointing and saccade task (T2*-weighted gradient echo planar imaging,

114   FOV = 24.0 cm, matrix = 80 x 80, in-plane resolution of 3mm, TR = 2 s, TE = 30 ms,

115   FA = 90°, 35 contiguous axial slices acquired in an interleaved order along the AC-PC

116   line). Visual stimuli were rear-projected using an LCD projector (NEC LT 265 DLP

117   projector; resolution, 1024 x 768; 60 Hz refresh rate) on a screen mounted behind

118   the participant, and viewed by the participant via a mirror mounted to the head coil

119   directly above the eyes. The visual presentation consisted of a circular arrangement

120   of 8 white circles (~15 degrees of visual angle) surrounding a central red or green

121   square (Figure 1). Participants were instructed to make self-paced centre-out

122   pointing movements to each white circle in the circular arrangement while fixating

123   on a central fixation square when it is red and execute centre-out saccades when the

124   central square is green. The intertrial interval was 2 s. In each movement block

125   (pointing and saccade conditions), participants started each respective centre-out

126   movement towards the 12 o'clock white circle and proceeded in a clockwise manner

127   until the end of the block. The reach-saccade localizer included 8 reaching blocks

128   (16 s per block), 8 saccade blocks (16 s per block), and 3 fixation/baseline blocks

129   (10 s per block), which were placed at the beginning, middle and end of the run. The

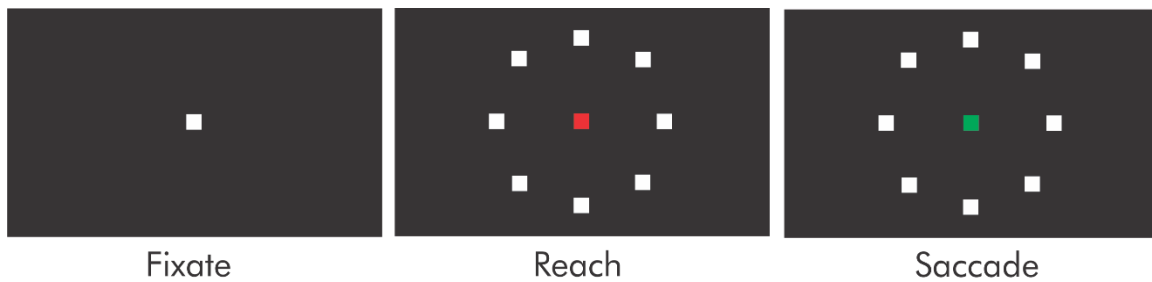130   localizer lasted 5 min 22 s (157 brain volumes).

131

Figure 1: Functional localizer task display. Participants performed the localizer task while laying supine inside the MRI. The visual stimuli were rear-projected using an LCD projector. Participants were instructed to fixate when the white square appears, and either perform centre-out reaches with the right hand or saccades when the white square turns respectively, red or green. Participants started each respective centre-out movement towards 12 o'clock and proceeded in a clockwise manner until the end of the block.

The functional localizer data were superimposed on the corresponding participant's high resolution anatomical image with an alignment on the AC-PC plane. All preprocessing and univariate analyses were performed using Brain Voyager QX version 2.6 (Brain Innovation). Preprocessing for the localizer data included slice scan-time correction, 3D motion correction (alignment of the first volume of the functional scan, which was closest in time, to the anatomical scan), high-pass temporal filtering of 3 cycles/run, functional-to-anatomical co-registration, and spatial smoothing (trilinear-sinc interpolation performed during realignment and sinc interpolation performed during reorientation). We contrasted BOLD signal for the pointing and fixation conditions rather than the pointing and saccade conditions to identify the hotspots of the left mIPS and left PMd due to known activation overlap in response to saccade and reach planning (Vesia et al., 2010). The left mIPS and left PMd were reliably identified in each participant by significantly higher response during the pointing condition compared to the fixation condition. The location of the left mIPS was defined by selecting the peak activity voxel or voxel

154   cluster medial to the intraparietal sulcus in the left hemisphere (Vingerhoets, 2014).

155   The location of the left PMd was defined by selecting the peak activity voxel or voxel

156   cluster at the junction of the precentral sulcus and the superior frontal sulcus in the

157   left hemisphere (Amiez, Kostopoulos, Champod, & Petrides, 2006).

158   **Co-registration**

159   The scalp location corresponding to the target cortical area was identified using

160   Brainsight (Rogue Research Inc., Montreal, Quebec) and marked to guide electrode

161   placement so that the peak electric field of HD-tDCS would be directed at the targeted

162   cortical area. The nasion, nose tip, left and right inter-tragal notches were used as

163   landmarks to guide participant-image registration, and the targets (peak voxel

164   representing the left mIPS and PMd) were selected as the foci for stimulation from the

165   superimposed functional image data. The marked location was the minimum inline

166   projection of the target mapped onto the scalp. The MNI coordinates of each intended site

167   of stimulation were recorded for comparisons with those reported in the literature. The

168   mean normalized MNI coordinates (±standard deviation [SD]) of the stimulation points

169   were -25 ± 5, -58 ± 6, and 52 ± 6 mm for the left mIPS and -25 ± 6, -9 ± 5, and 59 ± 5

170   mm for the left PMd (x, y, z), consistent with the locations reported in studies using

171   various approaches summarized in Table 1 (mIPS coordinates reported in fMRI studies:

172   Davare, Zenon, Pourtois, Desmurget, & Olivier, 2012; Grefkes, Ritzl, Zilles, & Fink,

173   2004; Prado et al., 2005; Stark & Zohary, 2008; Blangero, Menz, McNamara, &

174   Binkofski, 2009; mIPS coordinates used in TMS studies: Vesia, Prime, Yan, Sergio, &

175   Crawford, 2010; Davare, Zenon, Pourtois, Desmurget, & Olivier, 2012; PMd: Meta-

9

176   analysis of 31 studies, Mayka, Corcos, Leurgans, & Vaillancourt, 2006; PMd coordinates

177   reported in fMRI study: Gallivan, McLean, Smith, & Culham, 2011).

178

179   **Table 1.** MNI coordinates reported in studies using different approaches.

| Source	Approach	Region	x	y	z
Davare, Zenon, Pourtois, Desmurget, & Olivier, 2012	TMS	Left mIPS	−32 ± 5	−49 ± 6	46 ± 9
Grefkes, Ritzl, Zilles, & Fink, 2004	fMRI	Left mIPS	−28	−50	52
Present study		**Left mIPS**	**−25 ± 5**	**−58 ± 6**	**52 ± 6**
Mayka, Corcos, Leurgans, & Vaillancourt, 2006	Meta-analysis, ALE	Left PMd	−30	−4	58
Gallivan, McLean, Smith, & Culham, 2011	fMRI	Left PMd	−28 ± 3.9	−14 ± 4	53 ± 4.3
Present study			**−25 ± 6**	**−9 ± 5**	**59 ± 5**

180

181   **High-Definition Direct Current Stimulation**

182   Continuous direct current was generated by a microprocessor-controlled constant

183   current source (DC-STIMULATOR MC, NeuroConn GmbH, Ilmenau, Germany), and

184   delivered using sintered Ag/AgCl ring electrodes (1cm diameter) for 20 min at a

185   current strength of 2mA. The 4x1 electrode configuration was used and consisted of

186   a central electrode placed on marked position from co-registration, and surrounded

187   by four pick-up electrodes at a radius of 3 cm. To improve the conductance, hair was

188   washed and dried prior to the experiment, and separated under the scalp using

189   cotton swabs. Electrodes were stabilized within plastic holders filled with

190   conducting gel embedded in a mesh cap which was fastened on the participant's

191   head with straps. The impedance was under 20 kΩ throughout stimulation.

192   On separate days, anodal or cathodal stimulation were administered to the

193   left mIPS or the left PMd for a total of 4 sessions. At each site, the order of the

194   stimulation polarity was randomly counterbalanced across participants. Each

195   session consisted of three conditions, pre-stimulation (control), stimulation, and

196   post-stimulation and each participant completed 250 trials per condition (50 trials

197   per block x 5 blocks per condition), for a total of 750 trials per session (Figure 2).

198

	tDCS (anodal or cathodal)	
Pre 1 - 5 250 Trials	Stim 1 - 5 250 Trials (20 min)	Post 1 - 5 250 Trials

199
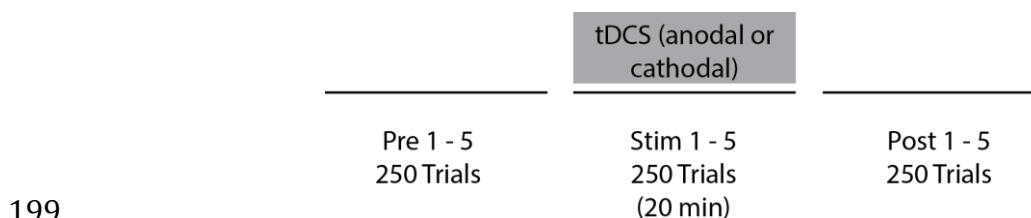
200   **Figure 2.** Schematic representation of the experimental protocol.
201   Pre blocks 1 - 5 were collected prior to stimulation to measure the participant's baseline performance for
202   that day. For stim blocks 1 - 5, anodal or cathodal tDCS was applied to either the left mIPS or the left PMd
203   for 20 min. After stimulation, post blocks 1-5 were collected to examine how tDCS-induced effects evolve
204   over time. EEG activity was collected in pre blocks 1-5 and post blocks 1-5.
205

206   **Experimental Setup**

207   Participants were seated in a dark room with their head immobilized in an upright

208   position by dental impressions attached to a tilted reaching setup, such that their

209   straight-ahead gaze aligned with a fixation cross (Figure 3). Visual stimuli (i.e.,

210   initial hand position, fixation cross, target) were presented on a tilted overhead

211   monitor and viewed in a tilted semi-silvered mirror located midway between the

212   tilted reaching surface and the monitor. All surfaces were tilted at 30°. Hand

213   position was occluded by the semi-silvered mirror but was displayed as a

214   representative visual marker to guide the initial alignment of the right index

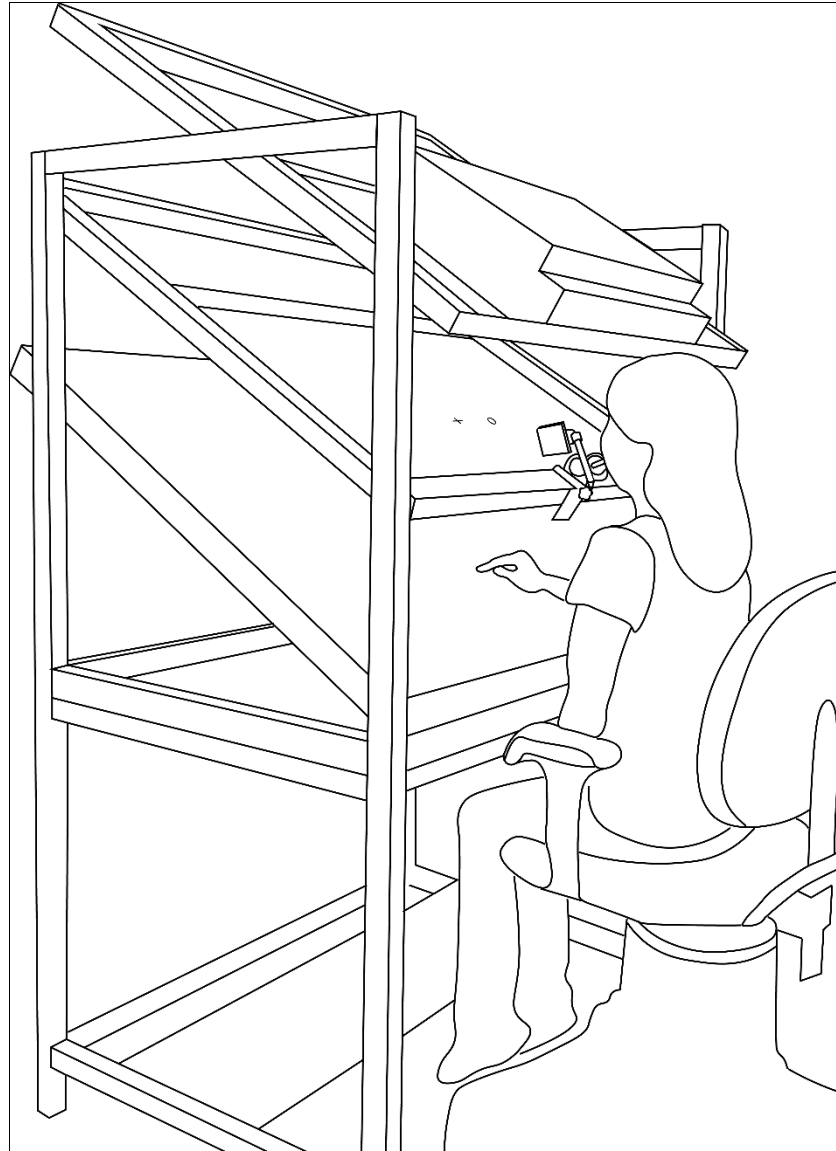215   fingertip to the starting position and extinguished at movement onset.

216
217
218 **Figure 3.** Schematic representation of experimental setup.
219 Participant is seated upright in front of a virtual reality set-up with their head immobilized by an individual
220 dental impression. Visual stimuli is presented on an overhead monitor and viewed in a semi-transparent
221 mirror, which allowed the reflected visual stimuli to be in the plane of the reaching surface.
222

223

224   Eye fixation was monitored using EyeLink 1000 eye tracking system (SR Research;

225   sampling rate, 500 Hz; accuracy, 0.5°). Hand movement data were obtained by

226   localizing the 3D position of infrared light-emitting diodes taped to the tip of the

227   right index finger (Optotrak Certus; Northern Digital; sampling rate, 400 Hz;

228   accuracy, 0.1 mm.

229   We recorded a measure of cortical excitability in the targeted cortical regions

230   using electroencephalography before and after stimulation. This set-up included V-

231   Amp 16, OpenViBE driver, Vamp-16 EEG amplifier (Brain Products), sintered

232   Ag/AgCl electrodes, a reference electrode attached to the skin surface above

233   participant's vertebrate C7 and a ground electrode attached to the elbow. This data

234   was not used for the following analyses.

235

236   **Reaching Task**

237   The reaching task required participants to make reaching movements from one of

238   2 initial hand positions (7.5cm left/right of midline) to one of 4 randomly chosen

239   briefly flashed targets (20cm distant, 5cm apart horizontally) while fixating on a

240   straight-ahead cross in-line with the targets. The trial began with the presentation

241   of a marker to direct the participant to the initial hand position (IHP). Upon aligning

242   the right index fingertip with the IHP, the IHP cue extinguished and a fixation cross

243   appeared (500 – 1000 ms after trial start), during which a target was briefly

244   presented. The participant was allowed to move immediately in response to the

245   brief presentation of the target and was instructed to maintain their gaze on the

246   fixation cross when the target flashed as well as during the reaching movement.

247   Reaching task display and timings are presented in Figure 4, and outlined above eye

248   position (Figure 5B), hand position (Figure 5C) and velocity plots (Figure 5D) for an

249   exemplary participant reach (Figure 5A). All target-directed reaches were

250   performed without visual feedback of the hand. Instructions and practice (10 trials)

251   were provided prior to the main task.

252
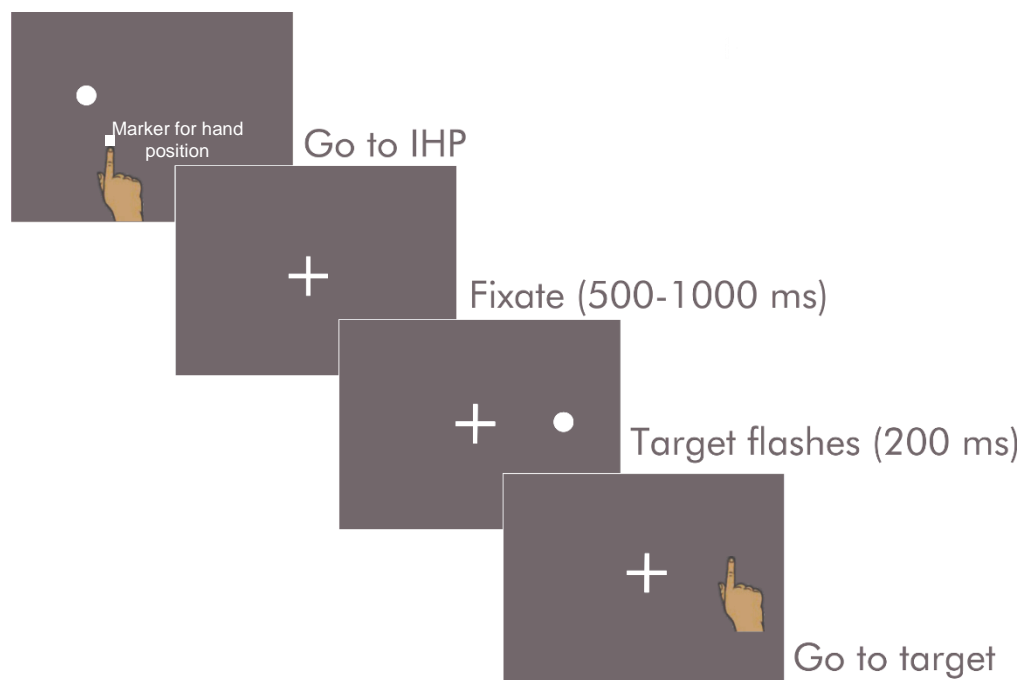
253

254   **Figure 4:** Reaching task display and timing.
255   A typical trial begins with the participant aligning their right index finger (indicated by a visible marker) to
256   the IHP cue. Vision of the hand is occluded by the semi-silvered mirror. However, the participant is
257   provided with a marker representing the hand position prior to target-directed reaching. A fixation cross
258   then appears, followed by the brief presentation of the target. The participant then moves immediately to
259   the target and the marker indicating hand position is extinguished at the onset of movement. Target viewing
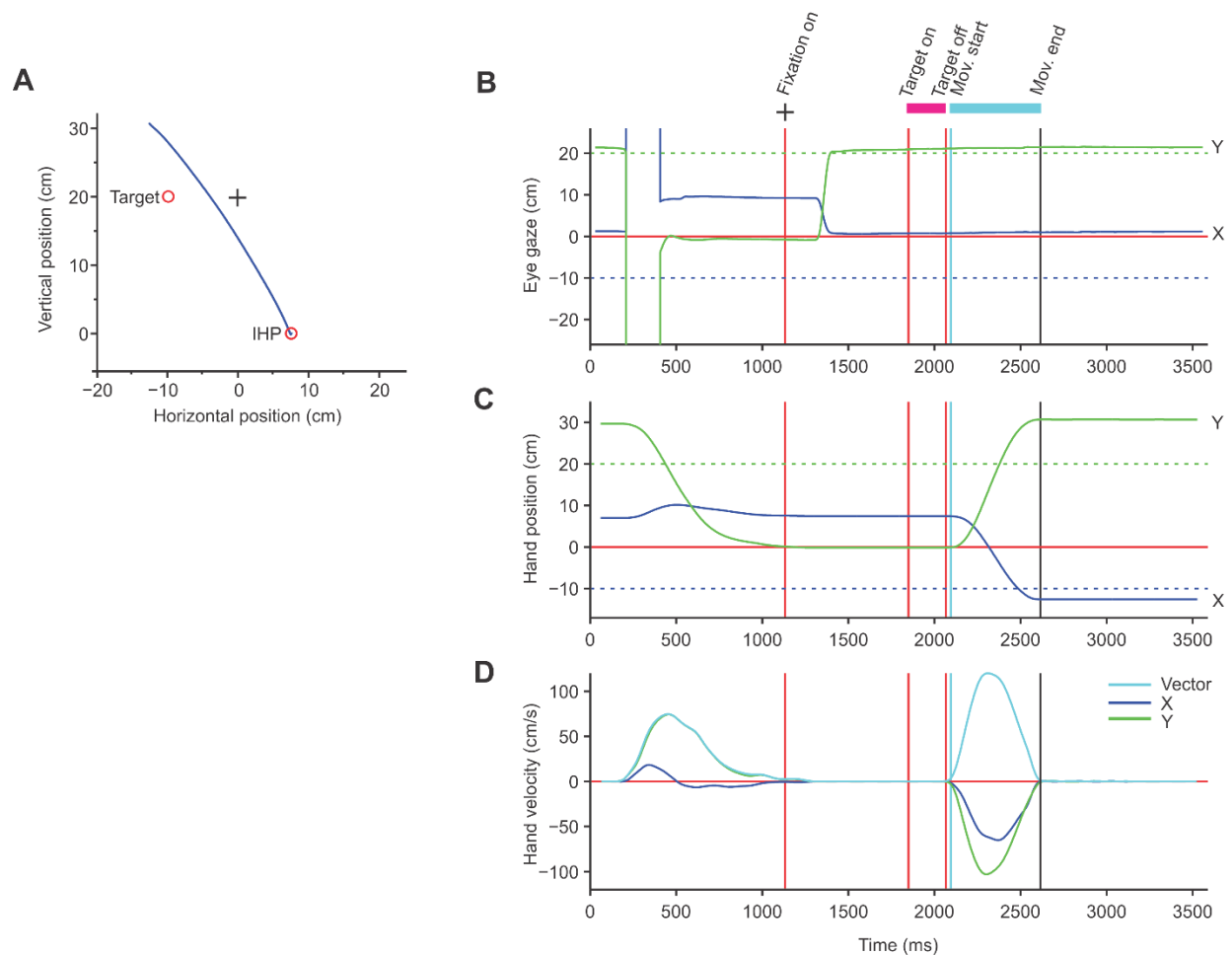260   and target-directed reaches are performed with peripheral vision.

Figure 5: Typical participant trial.
(A) Raw reaching trajectory from a typical trial. The required reach begins at the initial hand position, IHP, and ends at the target (red open circles). The blue line represents the participant's hand trajectory. In this trial, the participant starts the reach with an IHP offset to the right by 7.5 cm.
(B) Eye gaze traces. Horizontal (blue) and vertical (green) eye positions, from EyeLink recordings. Horizontal and vertical target position (dotted lines) are also plotted over time. Participants were instructed to keep the eyes fixated on the fixation cross (located at 0, 20 cm) throughout the trial. (C) Hand position traces. Horizontal (blue) and vertical (green) hand positions (solid lines) and horizontal and vertical target position (dotted lines) plotted over time. The trial begins when the subject aligns the fingertip indicator with the visual IHP and the simultaneous onset of the fixation cross. The fixation cross remains on until the end of the trial. The target then appears briefly. Participants were instructed to move in response to the flash of the target. Movement start and end times are represented by teal and black lines. (D) Hand velocity traces. Horizontal (blue), vertical (green), and vector (teal) hand velocities plotted over time.

15

Data analyses

Offline analyses were performed using MATLAB (The Mathworks, Natick, MA). We smoothed the movement data using a low-pass, auto-regressive forward-backward filter (cutoff of 50Hz, eye data; 25Hz, hand). We removed trials in which participants broke fixation (Figure 5B).

A threshold of 1cm/s determined the onset/completion of a reach. The horizontal and vertical endpoint error were defined as the horizontal and vertical components of the displacement of the reach endpoint with respect to the target location.

Repeated measures ANOVAs were performed on changes in horizontal and vertical endpoint error, with the 4 factors, target location (-10, -5, 5, 10 cm), IHP (-7.5, 7.5 cm), polarity (anodal, cathodal), and site of stimulation (left mIPS, left PMd) at each epoch (change from baseline, during and after stimulation). ANOVA statistics were corrected for inhomogeneity of variance using the Greenhouse-Geisser correction when the Mauchly's Test of Sphericity indicated that the assumption of sphericity had been violated. Three-way interactions were examined at each level of the fourth variable (site of stimulation), followed by two-way interactions at each level of the third variable (polarity). Interaction effects of IHP x target position, and/or main effects would indicate to us how the mIPS and PMd differ in their level of movement coding.

298 **Results**

299 Only the cathodal polarity and post-stimulation epoch combination produced

300 noticeable effects on horizontal endpoint error. Here, we focused on changes in

301 horizontal endpoint error when reaching toward targets from the left and right IHPs

302 after cathodal mIPS and PMd stimulation. Although the arrangement of the targets

303 in the reaching task was designed to examine horizontal endpoint errors, vertical

304 endpoint patterns also conformed to our interpretations (Figure S1, Appendix).

305

306 **Individual Participant Endpoint Error Analysis**

307 In individual participants (Figures 6 and 7), the change in reach endpoint pattern

308 following mIPS stimulation (gaze-centered expansion or contraction of reach

309 endpoints) depended on the IHP (left or right), while the endpoint pattern was IHP-

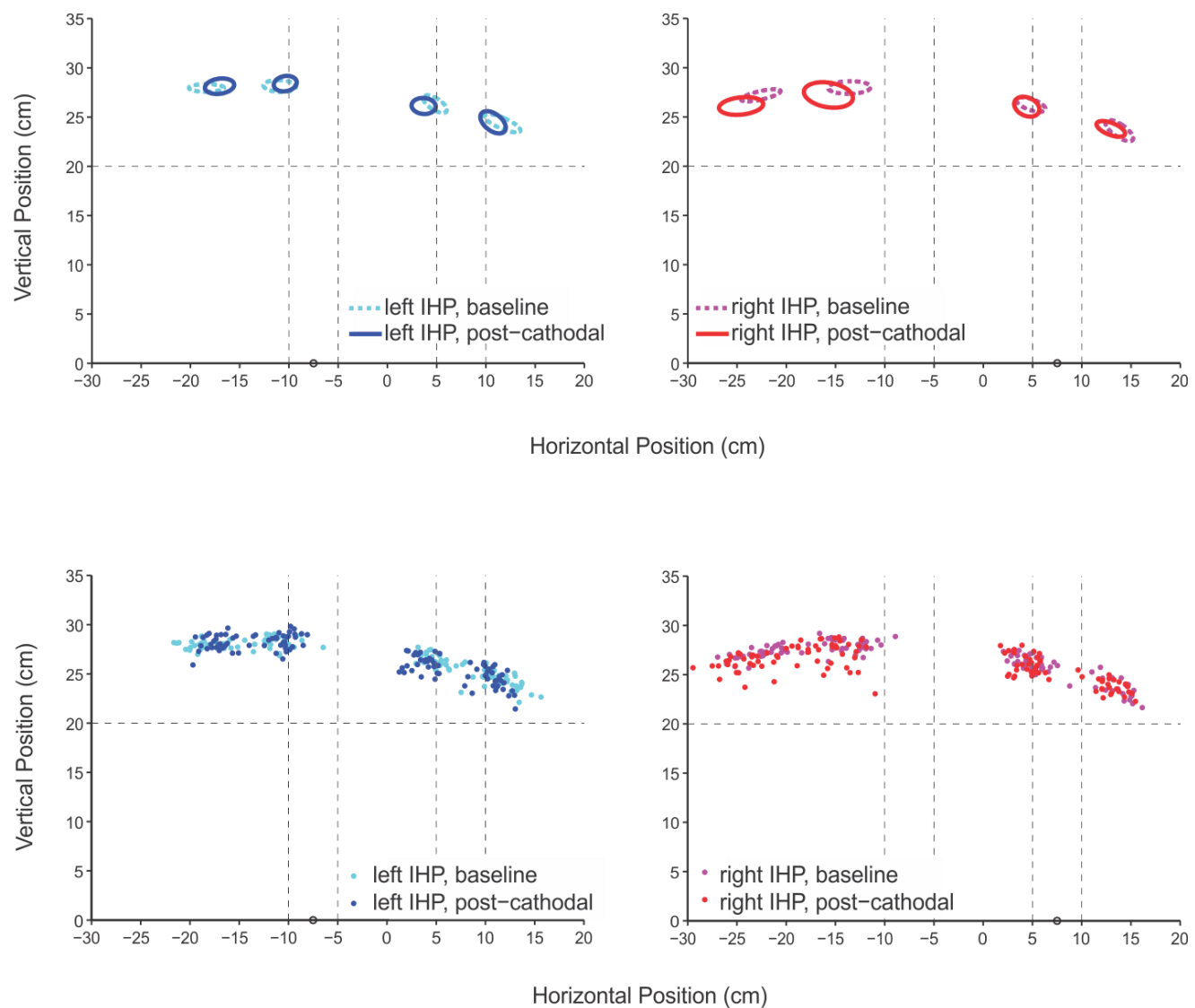310 independent following PMd stimulation (contraction of reach endpoints for both

311 IHP).

312 **Figure 6:** Reach endpoints pre- and post-cathodal mIPS stimulation.
313 Standard ellipses of reach endpoints for each target location, with individual reach endpoints shown
314 below, for all trials before (dotted teal and magenta) and after cathodal mIPS stimulation (solid blue
315 and red), separated into reaches starting from the left (blues) and right IHP (reds), from a
316 participant. The hand indicates the IHP and the intersections of the dashed guidelines represent
317 target locations. It appears that there is a horizontal contraction effect of stimulation on the
318 endpoints for reaches starting from the left IHP, but a horizontal expansion effect on the endpoints
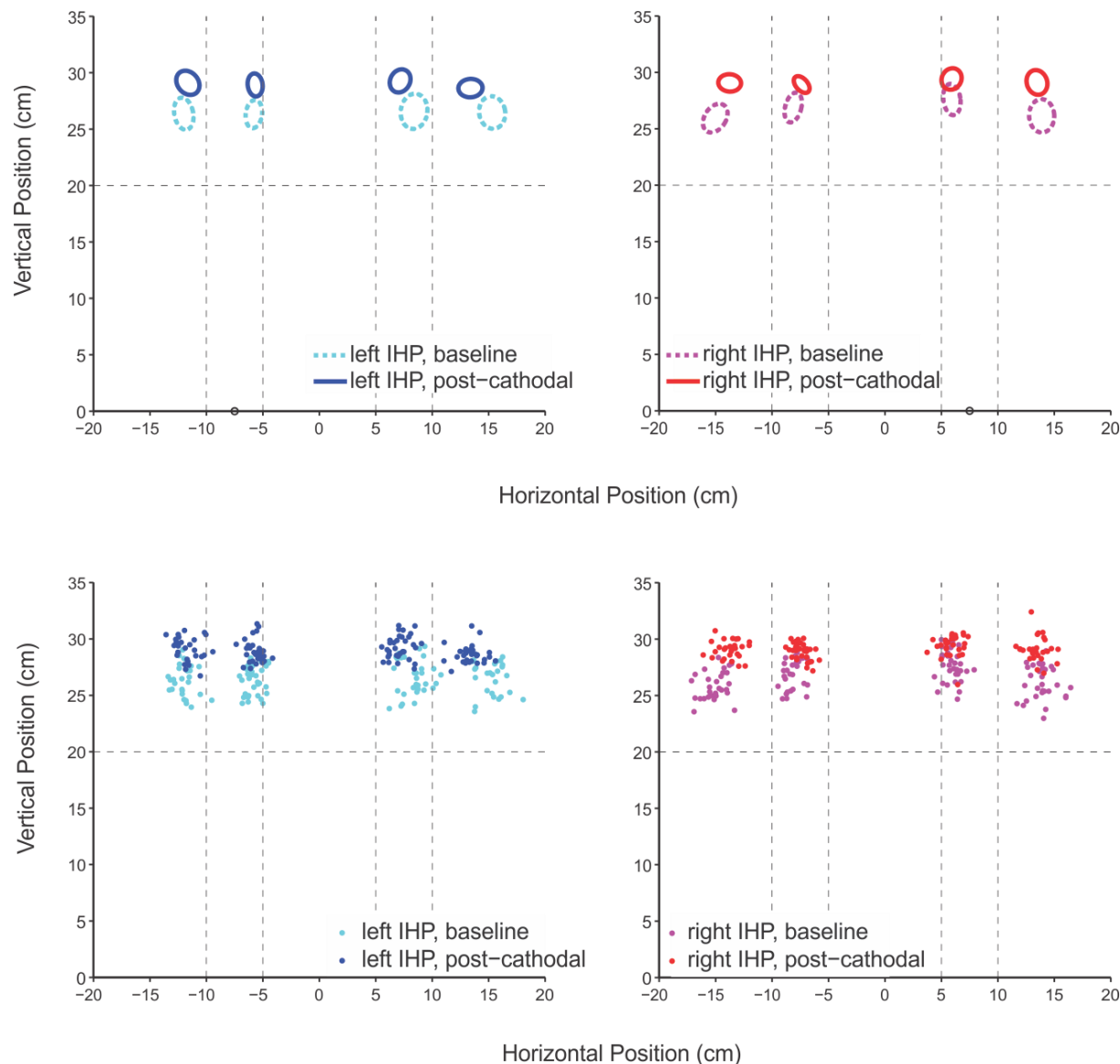319 for reaches starting from the right IHP.
320

18

Figure 7: Reach endpoints pre- and post-cathodal PMd stimulation.
Standard ellipses of reach endpoints for each target location, with individual reach endpoints shown below, for all trials before (dotted teal and magenta) and after cathodal PMd stimulation (solid blue and red), separated into reaches starting from the left (blues) and right IHP (reds), from a participant. The hand indicates the IHP and the intersections of the dashed guidelines represent target locations. It appears that there is a horizontal contraction effect of stimulation on the endpoints for reaches starting from either IHPs.

Group-level Endpoint Error Analysis

Two separate two-way repeated measures ANOVAs at the group-level with the

within-subject factors of IHP and target position on the change in horizontal error

19

333   post vs pre-cathodal stimulation for each stimulation site were conducted. The full

334   4-way RM-ANOVA with the within-participant factors IHP, target position, polarity,

335   and site revealed significant main target effect (F(3, 288) = 9.46, p = .0002),

336   target*site interaction effect (F(3, 288) = 3.94, p = .0188), target*IHP*polarity

337   interaction effect (F(3, 288) = 3.36, p = .0333), and IHP*polarity*site interaction

338   effect (F(1, 288) = 31.2, p = .0003). We followed up the significant interactions

339   consisting of the site term using separate 3-way RM-ANOVAs at each level of site,

340   with the within-participant factors, polarity, target, and IHP. We found significant

341   target*IHP*polarity interaction effect at the mIPS (F(3,144) = 4.26 , p = .0138), and

342   significant target main effect (F(3,144) = 13.8 , p < .0001) and IHP*polarity

343   interaction effect (F(1,144) = 4.07 , p = .0288) at the PMd. We then followed up the

344   significant interaction effects by conducting separate 2-way RM-ANOVAs at each

345   level of polarity. The significant interaction and main effects are illustrated in Figure

346   8. An RM-ANOVA of the left mIPS post-cathodal change in horizontal endpoint error

347   yielded a target x IHP interaction effect, *F*(3, 72) =3.31, *p* = .0350. A significant IHP

348   by target position interaction effect demonstrates that the pattern across target

349   positions differ according to IHP conditions (starting from the left or right) and

350   would support separate IHP and target position coding at the input of mIPS.

351   Contrastingly, at the left PMd, the RM-ANOVA yielded separate main effects of IHP,

352   *F*(1, 72) = 7.7, *p* = .0216 and target position, *F*(3, 72) = 7 , *p* = .0012, which support

353   IHP-independent modulation of the movement vector and therefore movement

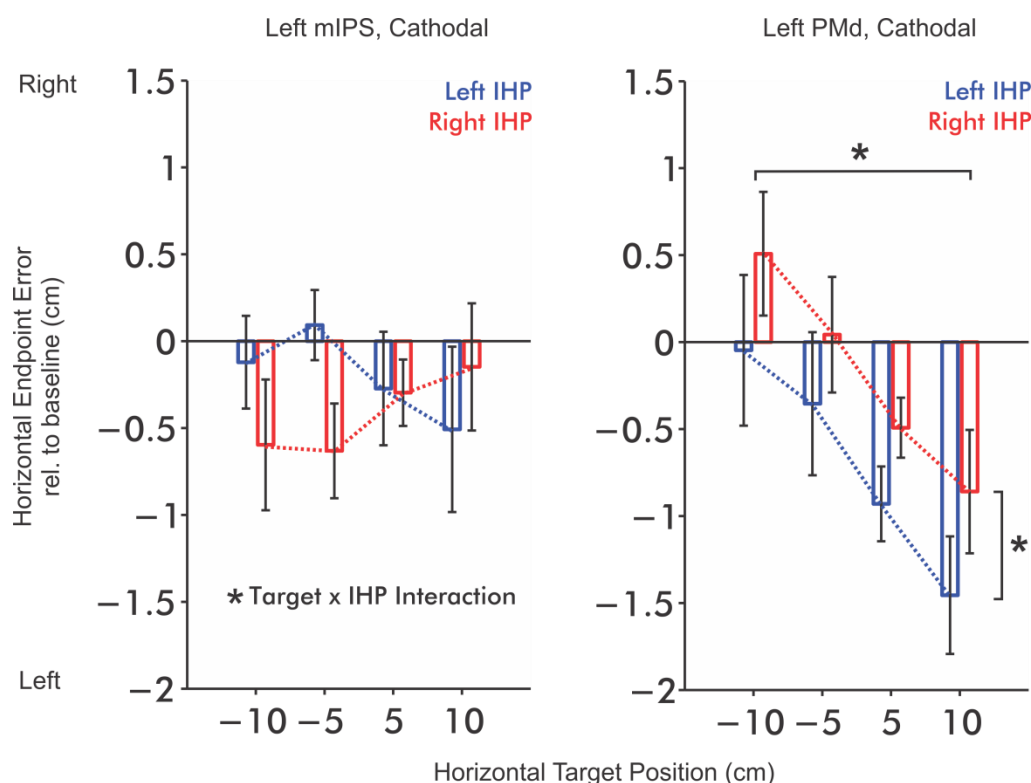354   vector coding at the input of PMd.

355

Figure 8: Group-level post-cathodal tDCS change in the horizontal endpoint error relative to baseline. Change in the horizontal component of reaching endpoint across target positions after cathodal stimulation of the left mIPS (left) and left PMd (right), separated according to left IHP (blue) and right IHP (red). Positive values represent endpoint falling to the right of the target and negative values represent endpoints falling to the left of the target. Error bars represent SEM. RM-ANOVAs of the post-cathodal change in horizontal endpoint error yielded a significant target x IHP interaction effect (* indicates p < .05) at the mIPS, suggesting independent IHP and target coding at the input of mIPS. Conversely, significant IHP and target main effects found at the PMd suggest that IHP and target position may be integrated into a movement vector code at the input of PMd.

Alternative Explanations

We considered alternative explanations such as differences in information

processing, speed-accuracy trade-offs, and feedback processes that could otherwise

explain our results. Reaction and movement times did not significantly differ

between conditions or between sessions (all *ps* > .05), therefore precluding the

likelihood of our results being driven by differences in information processing and

speed-accuracy trade-offs in movement execution. We did not find evidence of

course adjustment during the movement from the hand position and velocity

21

375   profiles (Figures S2 & S3, Appendix). Spatial trajectories were typically straight

376   without terminal hooks and average velocity profiles were symmetrical and single

377   peaked without additional valleys or inflections (Figure S4, Appendix), therefore

378   precluding the likelihood of corrective sub-movements. This is not unusual given

379   the lack of visual feedback. Thus, we do not have evidence to suggest that the

380   changes in error patterns resulted from disturbed online control.

381

Discussion

The current study is the first to apply HD-tDCS to directly investigate movement planning properties of the human mIPS and PMd. We found evidence that the mIPS receives independently coded target position and IHP information while the input of the PMd receives a vector-based movement plan. The present study demonstrates that the input of mIPS and PMd receive movement-relevant information at different levels of complexity towards the construction of a movement plan. Furthermore, we provide evidence that HD-tDCS can modulate performance in a movement planning task to support the understanding of the functional properties of mIPS and PMd.

Differences in horizontal error patterns were elicited from cathodal stimulation while that elicited from anodal stimulation were not significant. The mechanism that would explain the changes in behaviour resulting from cathodal stimulation is unlikely to be as straightforward as the general assumption of polarity-dependent modulation of excitability under the active electrode. Such an explanation would overlook the influence of the electrical field orientation across the convoluted cortical surface (Garnett, Malyutina, Datta, & den Ouden, 2015) which determines current direction with respect to the neuronal alignment and therefore the effect on neuronal excitability (Kabakov, Muller, Pascual-Leone, Jensen, & Rotenberg, 2012). Although the mechanism connecting excitability changes to behavioural changes has yet to be identified, the observable perturbations in movement errors permitted us to recognize how movement related components might be encoded at the input of the perturbed cortical areas.

404   The significant changes in movement errors produced by cathodal HD-tDCS

405   in the stimulation offset period which were absent during stimulation lines up with

406   the timeline of peak effects of the 4 x 1 HD-tDCS reported elsewhere, appearing not

407   immediately after stimulation but half an hour after the end of stimulation (Villamar

408   et al., 2013a; Villamar et al., 2013b; Kuo et al., 2013).

409   We observed behavioral changes in response to targeted HD-tDCS at the

410   mIPS and PMd that would be consistent with independently coded target position

411   and IHP by the former and dependent coding by the latter. The implications of this

412   study for the use of HD-tDCS as a research technique is that there is a positive

413   outlook for its use to clarify structure-function relationships in other brain areas

414   and cognitive domains. The value of HD-tDCS lies in the focality that make it

415   possible to target specific cortical areas. The validity of conclusions derived from

416   this technique could be further strengthened by a complete mechanistic

417   understanding of HD-tDCS.

418   In this study, we used a novel technique that distinguished the property of

419   signals carried at the input of mIPS and PMd. This sets apart our experiment from

420   TMS studies of the same areas where the effects are on the cortical output and

421   processing at sites receiving projections from the stimulated site (Siebner,

422   Hartwigsen, Kassuba, & Rothwell, 2009), whereas tDCS is thought to disrupt the

423   input of a stimulated area, specifically, the presynaptic activity of stimulated

424   neurons (Bączyk & Jankowska, 2014).

425   Together, the results of the two techniques assembles an overall picture of

426   vector formation. Separably-encoded representations of the IHP and target position

427   are provided at the input of mIPS and combined prior to the output of the mIPS.

428   Together the present study and TMS literature closes in on mIPS as a location where

429   vector formation occurs. For that reason, our results are complementary to rather

430   than at odds with previous literature on the mIPS that proposed vector-based

431   representation of the movement plan in the mIPS (Davare, Zénon, Desmurget, &

432   Olivier, 2015; Vesia, Prime, Yan, Sergio, & Crawford, 2010). Our results about the

433   PMd are also compatible with monkey neurophysiological and TMS findings that

434   support a vector-based movement plan in the PMd (Kurata, 1993; Fu, Flament,

435   Coltz, & Ebner, 1995; Davare, Zénon, Desmurget, & Olivier, 2015).

436

Conclusion

438   Our results provide a plausible picture of where and how spatial information about

439   the target position and IHP may be incorporated into a movement plan. The

440   continued use and scientific acceptance of this exploratory tool for investigating the

441   specific function of brain areas would benefit from identification of the mechanism

442   in which HD-tDCS operates.

443

444

Acknowledgements

References

451

452 Amiez, C., Kostopoulos, P., Champod, A.-S., & Petrides, M. (2006). Local morphology predicts

453   functional organization of the dorsal premotor region in the human brain. The Journal of

454   Neuroscience: The Official Journal of the Society for Neuroscience, 26(10), 2724–2731.

455   https://doi.org/10.1523/JNEUROSCI.4739-05.2006

456 Bączyk, M., & Jankowska, E. (2014). Presynaptic actions of transcranial and local direct current

457   stimulation in the red nucleus: Presynaptic modulation. The Journal of Physiology,

458   592(19), 4313–4328.

459 Batista, A. P., Buneo, C. A., Snyder, L. H., & Andersen, R. A. (1999). Reach plans in eye-

460   centered coordinates. Science, 285(5425), 257–260.

461 Bindman, L. J., Lippold, O. C., & Redfearn, J. W. (1962). Long-lasting changes in the level of the

462   electrical activity of the cerebral cortex produced by polarizing currents. Nature, 196,

463   584–585.

464 Blangero, A., Menz, M. M., McNamara, A., & Binkofski, F. (2009). Parietal modules for

465   reaching. Neuropsychologia, 47(6), 1500–1507.

466 Bock, O., & Arnold, K. (1992). Motor control prior to movement onset: Preparatory mechanisms

467   for pointing at visual targets. Experimental Brain Research, 90(1), 209–216.

468 Cisek, P. (2002). Neural Activity in Primary Motor and Dorsal Premotor Cortex In Reaching

469   Tasks With the Contralateral Versus Ipsilateral Arm. Journal of Neurophysiology, 89(2),

470   922–942.

471 Datta, A., Bansal, V., Diaz, J., Patel, J., Reato, D., & Bikson, M. (2009). Gyri-precise head model

472   of transcranial direct current stimulation: Improved spatial focality using a ring electrode

473   versus conventional rectangular pad. Brain Stimulation, 2(4), 201–207.

474   Datta, A., Truong, D., Minhas, P., Parra, L. C., & Bikson, M. (2012). Inter-individual variation

475   during transcranial direct current stimulation and normalization of dose using MRI

476   derived computational models. Frontiers in Psychiatry, 3, 91.

477   Davare, M., Zénon, A., Desmurget, M., & Olivier, E. (2015). Dissociable contribution of the

478   parietal and frontal cortex to coding movement direction and amplitude. Frontiers in

479   Human Neuroscience, 9, 241.

480   Davare, M., Zenon, A., Pourtois, G., Desmurget, M., & Olivier, E. (2012). Role of the medial part

481   of the intraparietal sulcus in implementing movement direction. Cerebral Cortex, 22(6),

482   1382–1394.

483   Fu, Q. G., Flament, D., Coltz, J. D., & Ebner, T. J. (1995). Temporal encoding of movement

484   kinematics in the discharge of primate primary motor and premotor neurons. Journal of

485   Neurophysiology, 73(2), 836–854.

486   Gallivan, J. P., McLean, D. A., Smith, F. W., & Culham, J. C. (2011). Decoding effector

487   dependent and effector-independent movement intentions from human parieto-frontal

488   brain activity. Journal of Neuroscience, 31(47), 17149–17168.

489   Grefkes, C., Ritzl, A., Zilles, K., & Fink, G. R. (2004). Human medial intraparietal cortex

490   subserves visuomotor coordinate transformation. NeuroImage, 23(4), 1494–1506.

491   Jeannerod M, Arbib MA, Rizzolatti G, Sakata H. (1995). Grasping objects: the cortical

492   mechanisms of visuomotor transformation. Trends Neuroscience, 18, 314–320.

493   Krakauer, J. W., Pine, Z. M., Ghilardi, M. F., & Ghez, C. (2000). Learning of visuomotor

494   transformations for vectorial planning of reaching trajectories. The Journal of

495   Neuroscience, 20(23), 8916–8924.

496   Kuo, H.-I., Bikson, M., Datta, A., Minhas, P., Paulus, W., Kuo, M.-F., & Nitsche, M. A. (2013).

497   Comparing cortical plasticity induced by conventional and high-definition 4 Å~ 1 ring

498   tDCS: A neurophysiological study. Brain Stimulation, 6(4), 644–648.

499   Kurata, K. (1993). Premotor cortex of monkeys: set- and movement-related activity reflecting

500   amplitude and direction of wrist movements. Journal of Neurophysiology, 69(1), 187–

501   200.

502   Mayka, M. A., Corcos, D. M., Leurgans, S. E., & Vaillancourt, D. E. (2006). Three-dimensional

503   locations and boundaries of motor and premotor cortices as defined by functional brain

504   imaging: a meta-analysis. NeuroImage, 31(4), 1453–1474.

505   Prado, J., Clavagnier, S., Otzenberger, H., Scheiber, C., Kennedy, H., & Perenin, M.-T. (2005).

506   Two cortical systems for reaching in central and peripheral vision. Neuron, 48(5), 849–

507   858.

508   Purpura, D. P., & Mcmurtry, J. G. (1965). Intracellular activities and evoked potential changes

509   during polarization of motor cortex. Journal of Neurophysiology, 28, 166–185.

510   Siebner, H. R., Hartwigsen, G., Kassuba, T., & Rothwell, J. C. (2009). How does transcranial

511   magnetic stimulation modify neuronal activity in the brain? Cortex, 45(9), 1035–1042.

512   Stark, A., & Zohary, E. (2008). Parietal mapping of visuomotor transformations during human

513   tool grasping. Cerebral Cortex, 18(10), 2358–2368.

514   Vesia, M., Prime, S. L., Yan, X., Sergio, L. E., & Crawford, J. D. (2010). Specificity of human

515   parietal saccade and reach regions during transcranial magnetic stimulation. Journal of

516   Neuroscience, 30(39), 13053–13065.

517   Villamar, M. F., Volz, M. S., Bikson, M., Datta, A., Dasilva, A. F., & Fregni, F. (2013).

518   Technique and considerations in the use of 4x1 ring high-definition transcranial direct

519   current stimulation (HD-tDCS). Journal of Visualized Experiments: JoVE, (77), e50309.

520   Villamar, M. F., Wivatvongvana, P., Patumanond, J., Bikson, M., Truong, D. Q., Datta, A., &

521   Fregni, F. (2013). Focal modulation of the primary motor cortex in fibromyalgia using

522   4Å~1-ring high-definition transcranial direct current stimulation (HD-tDCS): immediate

523   and delayed analgesic effects of cathodal and anodal stimulation. The Journal of Pain,

524   14(4), 371–383.

525   Vindras, P., & Viviani, P. (1998). Frames of reference and control parameters in visuomanual

526   pointing. Journal of Experimental Psychology, 24(2), 569–591.

527   Vingerhoets, G. (2014). Contribution of the posterior parietal cortex in reaching, grasping, and

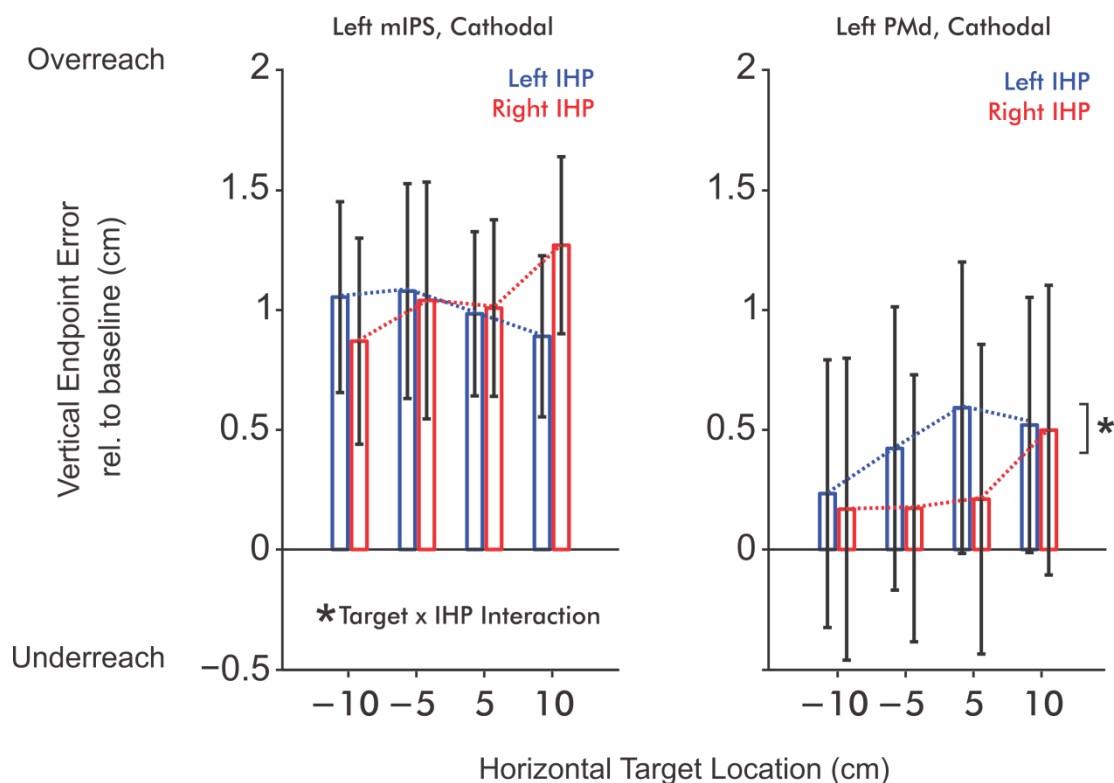528   using objects and tools. Frontiers in Psychology, 5.

529

Appendix
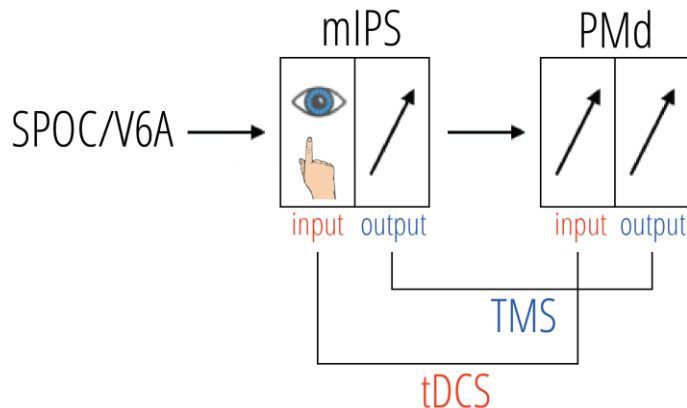

Figure 9: The model of the dorsomedial pathway we propose illustrates that the representation of the target position and IHP are separate at the input of the mIPS but are integrated into a vector representation at the input of the PMd.

Figure S1: Group-level post-cathodal tDCS change in the vertical endpoint error relative to baseline. Change in the vertical component of reaching endpoint across target positions after cathodal stimulation of the left mIPS (left) and left PMd (right), separated according to left IHP (blue) and right IHP (red). Positive values indicate that the endpoint falls relative to the target, farther away from the participant while negative values, closer to participant. Error bars represent SEM. Similar to the results of horizontal endpoint error, RM-ANOVA yielded a significant target by IHP interaction (* indicates $p < .05$) at the mIPS. However, only a IHP main effect was found at the left PMd.

31

544
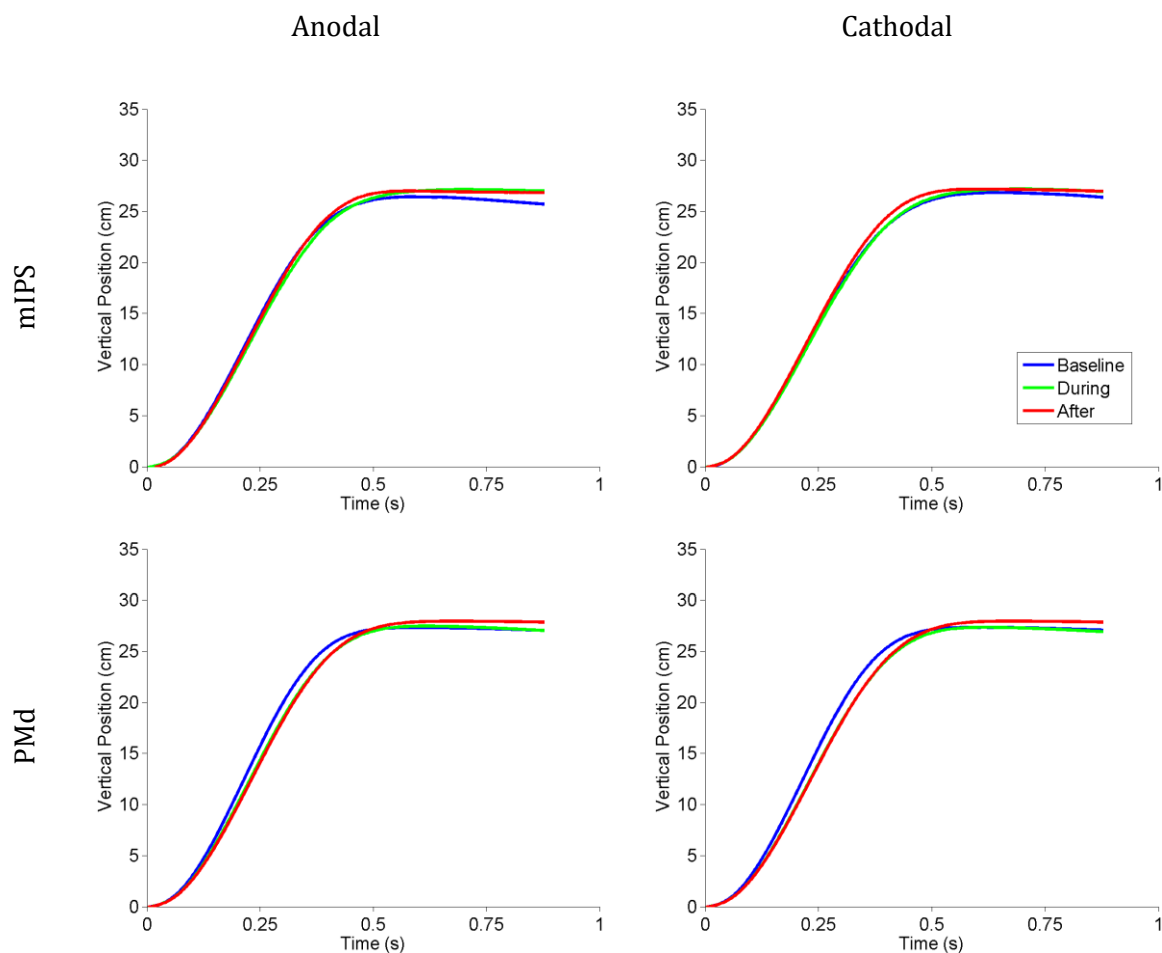
Figure S2: Average reaching position profiles.
Average position along the near-far axis for a representative participant, for equal distance reaches (towards targets located in the same hemifield as the IHP), before, during and after anodal and cathodal mIPS and PMd tDCS. The position profiles along the near-far axis were nearly identical across conditions.
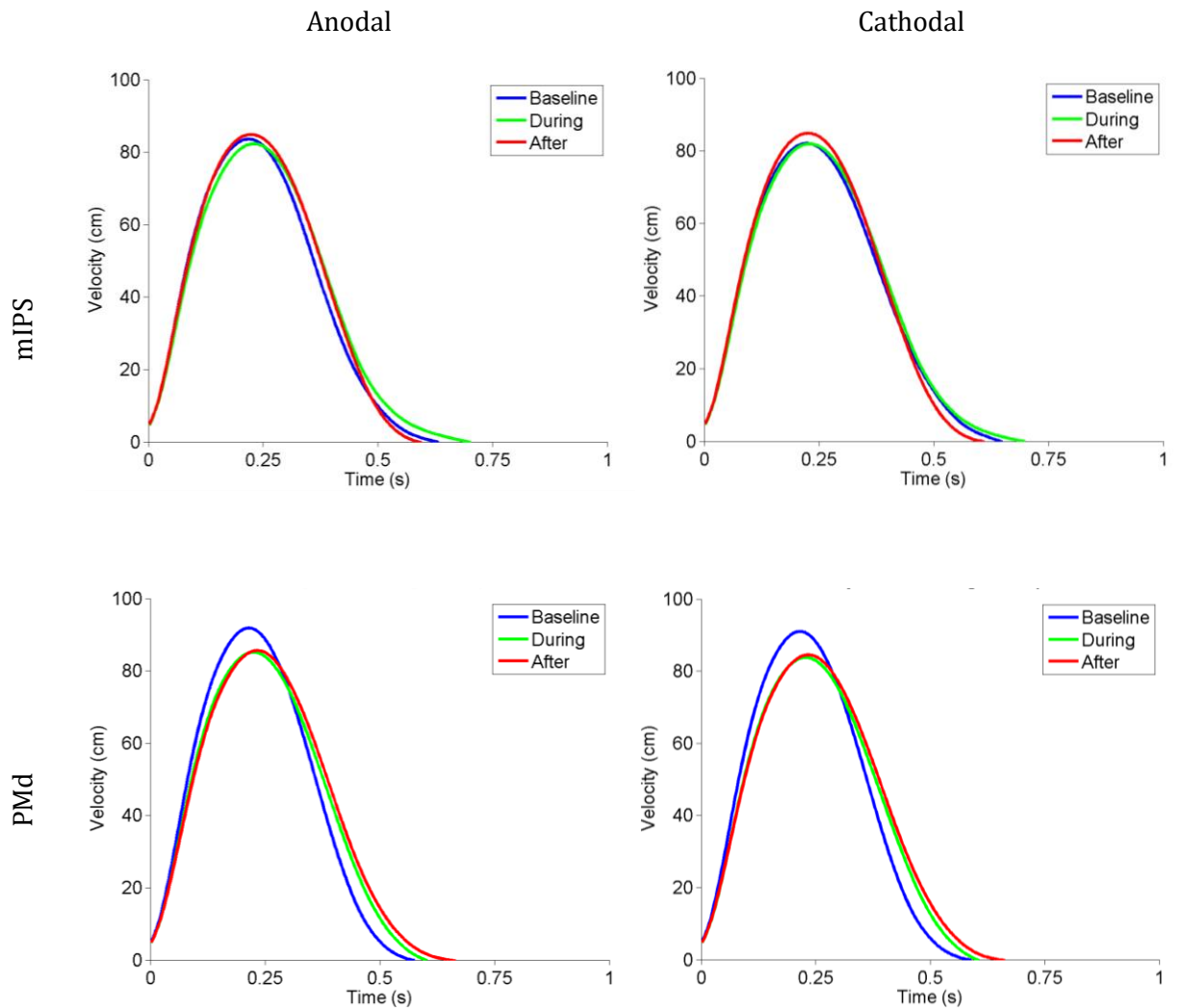
552

553

554 **Figure S3:** Average velocity profiles.
555 Average hand velocities of a typical participant for equal distance reaches (towards targets located in
556 the same hemifield as the IHP), before, during and after anodal and cathodal mIPS and PMd tDCS. The
557 velocity profiles along the near-far axis were nearly identical across conditions.
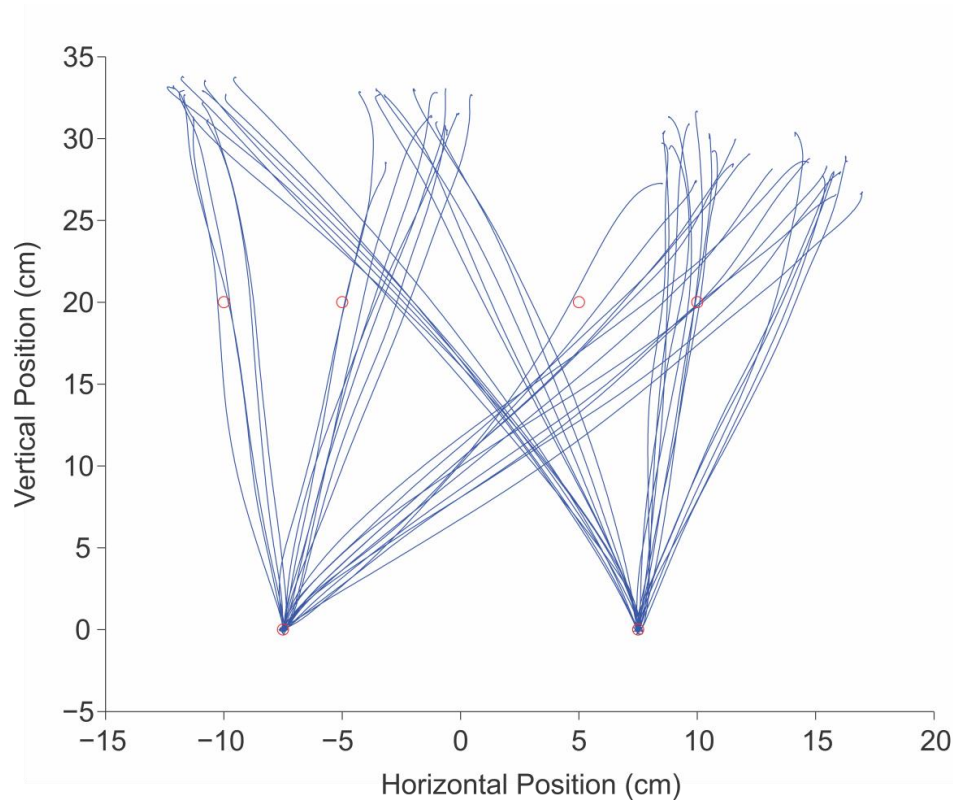558

559

560

Figure S4: Reaching trajectories.
Baseline trajectories made by an exemplary participant (P3) towards all targets starting from both
IHPs for one block of trials, shown in blue lines. Red circles indicate starting hand positions (-7.5, 7.5
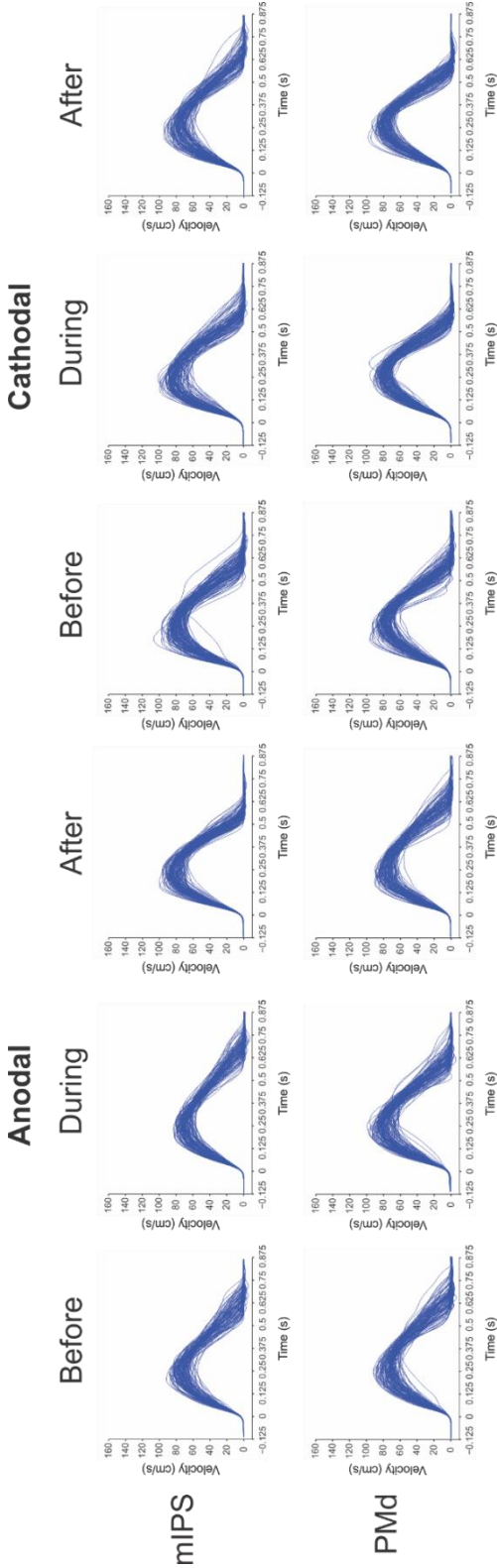cm from midline) and target positions (-10, -5, 5, 10 cm from midline, 20 cm distant).

566

Figure S5: Velocity profiles of a representative participant.
Velocity profiles before, during, and after anodal and cathodal tDCS of mIPS and PMd. Each line represents the velocity over time for a single trial. No additional valleys or inflections were observed in the individual trials to indicate the occurrence of sub-movements.

567
568

569 **Table S1.** Mean reaction time (+/- SE).
570 Mean reaction times at baseline, during and after anodal and cathodal mIPS and PMd stimulation epochs.

	Anodal						Cathodal					
	Before		During		After		Before		During		After	
	Mean	SE	Mean	SE	Mean	SE	Mean	SE	Mean	SE	Mean	SE
mIPS	277.45	12.68	266.82	9.55	265.16	11.4	288.55	19.49	276.01	16.27	273.63	17.23
PMd	286.83	17.49	276.95	15.69	262.62	13.76	301.17	24.57	295.21	33.46	294.13	31.79

571

572 **Table S2.** Mean movement time (+/- SE).
573 Mean movement time at baseline, during and after anodal and cathodal mIPS and PMd stimulation epochs.

	Anodal						Cathodal					
	Before		During		After		Before		During		After	
	Mean	SE	Mean	SE	Mean	SE	Mean	SE	Mean	SE	Mean	SE
mIPS	613.9	39.34	582.4	28.35	560.4	22.05	587.5	25.28	583.0	25.94	587.1	27.16
PMd	583.2	32.85	588.45	27.95	582.5	26.48	598.0	30.46	587.9	22.92	575.3	21.13

574
575

36

576 **Table S3:** Results of 2-way RM-ANOVAs on the change in horizontal and vertical endpoint error, during
577 and after anodal tDCS relative to baseline.
578 Bolded represents significant effects at p < .05.
579

Anodal	Horizontal	Vertical
During mIPS	**Target, F(3, 72)=8.74, p = .0003** IHP, F(1,72) = .76 , p = .4067 Targ* IHP, F(3, 72) =.65 , p = .5902	Target, F(3, 72) =1.9, p = .1529 IHP, F(1,72) =1.65 , p = .2316 Targ* IHP, F(3, 72) = .02 , p =.9947
After mIPS	**Target, F(3, 72) = 4.27, p = .0137** IHP, F(1,72) =3.2 , p = .1072 Targ* IHP, F(3, 72) = 1.18, p = .3353	Target, F(3, 72) =1.28, p = .3003 IHP, F(1,72) = .79, p = .3964 Targ* IHP, F(3, 72) =.6 , p = .6195
During PMd	Target, F(3, 72)=2.77, p = .0608 IHP, F(1,72) =1.15 , p = .3116 Targ* IHP, F(3, 72) = 1.55, p = .2236	**Target, F(3, 72)=5.64, p = .0039** IHP, F(1,72) =1.01 , p = .3422 Targ* IHP, F(3, 72) =2.18 , p = .114
After PMd	**Target, F(3, 72)=3.55, p =.0276** IHP, F(1,72) =.88 , p = .3718 Targ* IHP, F(3, 72) = 1.76, p = .178	**Target, F(3, 72)= 3.85, p =.0205** IHP, F(1,72) =0 , p = .9885 Targ* IHP, F(3, 72) =.55 , p = .6508

580
581
582 **Table S4:** Results of 2-way RM-ANOVAs on the change in horizontal and vertical endpoint error, during
583 and after cathodal tDCS relative to baseline.
584 Bolded represents significant effects at p < .05.
585

Cathodal	Horizontal Error	Vertical Error
During mIPS	Target, F(3, 72) = .06 , p = .982 IHP, F(1,72) =1.78 , p = .2152 Targ* IHP, F(3, 72) =2.25 , p = .1056	Target, F(3, 72)=.37, p = .7737 IHP, F(1,72) =.35 , p = .566 Targ* IHP, F(3, 72) =1.51 , p = .2351
After mIPS	Target, F(3, 72)=.02, p = .9955 IHP, F(1,72) =1.2 , p = .3015 **Targ* IHP, F(3, 72) =3.31 , p = .035**	Target, F(3, 72) = .27, p = .8457 IHP, F(1,72) =.12 , p = .7399 **Targ* IHP, F(3, 72) =3.92 , p = .0192**
During PMd	**Target, F(3, 72)=3.84, p = .0207** **IHP, F(1,72) = 6.55, p = .0307** Targ* IHP, F(3, 72) = .63, p = .6042	Target, F(3, 72)= 2.93, p = .0516 **IHP, F(1,72) = 6.58, p = .0304** Targ* IHP, F(3, 72) = 1.55, p = .2255
After PMd	**Target, F(3, 72) = 7, p = .0012** **IHP, F(1, 72) = 7.7, p = .0216** Targ * IHP, F(3, 72) = .04, p = .8619	Target, F(3, 72)= 1.86, p = .1605 **IHP, F(1,72) = 8.04, p = .0195** Targ* IHP, F(3, 72) = .98 , p = .4175

586
587

Table S5: Curvature parameters during and after anodal and cathodal tDCS relative to baseline. CAR = the curvature-to-amplitude ratio, DIR = initial movement direction (at 200 ms), and Θ, the angle at maximum curvature. None significant at alpha of .05.

Anodal	CAR	DIR	Θ
mIPS, during	Target, F(3, 72) = .2, p = .894 IHP, F(1,72) = .18, p = .6802 Targ* IHP, F(3, 72) = .17, p = .9155	Target, F(3, 72) = .05, p = .985 IHP, F(1,72) = .06, p = .8146 Targ* IHP, F(3, 72) = .02, p = .9957	Target, F(3, 72) = .05, p = .9833 IHP, F(1,72) = 0, p = .996 Targ* IHP, F(3, 72) = .53, p = .6675
mIPS, after	Target, F(3, 72) = 1.41, p = .2626 IHP, F(1,72) = .2, p = .669 Targ* IHP, F(3, 72) = .26, p = .8506	Target, F(3, 72) = .29, p = .8341 IHP, F(1,72) = .27, p = .6127 Targ* IHP, F(3, 72) = .36, p = .7805	Target, F(3, 72) = .53, p = .6653 IHP, F(1,72) = 0, p = .9986 Targ* IHP, F(3, 72) = .6, p = .6235
PMd, during	Target, F(3, 72) = 1.15, p = .3451 IHP, F(1,72) = 1.76, p = .2174 Targ* IHP, F(3, 72) = .65, p = .5899	Target, F(3, 72) = .73, p = .5404 IHP, F(1,72) = 1.82, p = .2106 Targ* IHP, F(3, 72) = 2.32, p = .0977	Target, F(3, 72) = 2.12, p = .1211 IHP, F(1,72) = .43, p = .5283 Targ* IHP, F(3, 72) = .78, p = .513
PMd, after	Target, F(3, 72) = 1.37, p = .274 IHP, F(1,72) = 1.24, p = .2951 Targ* IHP, F(3, 72) = .86, p = .4732	Target, F(3, 72) = .7, p = .5596 IHP, F(1,72) = .31, p = .5893 Targ* IHP, F(3, 72) = .65, p = .5926	Target, F(3, 72) = 1.06, p = .3831 IHP, F(1,72) = .49, p = .5031 Targ* IHP, F(3, 72) = .8, p = .5035
Cathodal	CAR	DIR	Θ
mIPS, during	Target, F(3, 72) = 1.24, p = .3154 IHP, F(1,72) = 0, p = .99446 Targ* IHP, F(3, 72) = 2.46, p = .0844	Target, F(3, 72) = 1.57, p = .2195 IHP, F(1,72) = .09, p = .7724 Targ* IHP, F(3, 72) = 1.37, p = .2737	Target, F(3, 72) = 1.83, p = .1648 IHP, F(1,72) = .11, p = .7442 Targ* IHP, F(3, 72) = 2.73, p = .0634
mIPS, after	Target, F(3, 72) = .6, p = .6189 IHP, F(1,72) = .15, p = .7051 Targ* IHP, F(3, 72) = 2.32, p = .0982	Target, F(3, 72) = .69, p = .568 IHP, F(1,72) = .32, p = .5878 Targ* IHP, F(3, 72) = 2.64, p = .07	Target, F(3, 72) = .73, p = .5438 IHP, F(1,72) = .11, p = .7442 Targ* IHP, F(3, 72) = 2.83, p = .0569
PMd, during	Target, F(3, 72) = 1.71, p = .1886 IHP, F(1,72) = .06, p = .8105 Targ* IHP, F(3, 72) = .61, p = .6149	Target, F(3, 72) = 1.5, p = .2377 IHP, F(1,72) = .93, p = .3603 Targ* IHP, F(3, 72) = .04, p = .9886	Target, F(3, 72) = 2.49, p = .0818 IHP, F(1,72) = 2.28, p = .165 Targ* IHP, F(3, 72) = .26, p = .8551
PMd, after	Target, F(3, 72) = 1.61, p = .2109 IHP, F(1,72) = .02, p = .8829 Targ* IHP, F(3, 72) = .48, p = .6984	Target, F(3, 72) = 2.39, p = .0903 IHP, F(1,72) = .32, p = .5849 Targ* IHP, F(3, 72) = .82, p = .4942	Target, F(3, 72) = 2.72, p = .064 IHP, F(1,72) = .2, p = .6632 Targ* IHP, F(3, 72) = .46, p = .7105

594 **Table S6:** Comparisons between curvature parameters before, during, and after anodal and cathodal tDCS.
595 CAR = the curvature-to-amplitude ratio, DIR = initial movement direction (at 200 ms), and ϴ, the
596 angle at maximum curvature. None significant at alpha of .05.
597

CAR	Comparison		Difference between estimated group means	Lower bound of 95% confidence interval for true mean difference	Upper bound of 95% confidence interval for true mean difference	p-value
	Pre-anodal	During	.0004	-.0077	.0085	.9992
	Pre-anodal	Post-anodal	-.0007	-.0087	.0074	.9964
	During	Post-anodal	-.0010	-.0091	.0070	.9856
	Pre-cathodal	During	-.0052	-.0157	.0054	.5647
	Pre-cathodal	Post-cathodal	-.0072	-.0178	.0033	.2744
	During	Post-cathodal	-.0021	-.0127	.0085	.9522

598

DIR	Comparison		Difference between estimated group means	Lower bound of 95% confidence interval for true mean difference	Upper bound of 95% confidence interval for true mean difference	p-value
	Pre-anodal	During	-.0975	-.3617	.1667	.7563
	Pre-anodal	Post-anodal	-.1878	-.4520	.0763	.2426
	During	Post-anodal	-.0903	-.3545	.1738	.7960
	Pre-cathodal	During	-.0975	-.3617	.1667	.7563
	Pre-cathodal	Post-cathodal	-.1878	-.4520	.0763	.2426
	During	Post-cathodal	-.0903	-.3545	.1738	.7960

599

ϴ	Comparison		Difference between estimated group means	Lower bound of 95% confidence interval for true mean difference	Upper bound of 95% confidence interval for true mean difference	p-value
	Pre-anodal	During	-.7134	-2.1305	.7037	.5381
	Pre-anodal	Post-anodal	-.9394	-2.3564	.4777	.3000
	During	Post-anodal	-.2260	-1.6430	1.1911	.9734
	Pre-cathodal	During	-.7134	-2.1305	.7037	.5381
	Pre-cathodal	Post-cathodal	-.9394	-2.3564	.4777	.3000
	During	Post-cathodal	-.2260	-1.6430	1.1911	.9734

600
601

602
603

40